Springer

KSME

Journal of Mechanical Science and Technology 29 (4) (2015) 1537~1545
www.springerlink.com/content/1738-494x
DOI 10.1007/s12206-015-0326-4

Prediction method for steady-state response of local rubbing blade-rotor systems †

Qian Zhao, Hongliang Yao*, Qi Xu and Bangchun Wen

School of Mechanical Engineering and Automation, Northeastern University, Shenyang, 110819, China

(Manuscript Received August 19, 2014; Revised December 15, 2014; Accepted December 23, 2014)

Abstract

Blade-rotor systems frequently encounter the problem of blade-to-case rubbing, which affects their safety and stability. Numerical simulation can be used to predict the steady-state response of these systems. However, such simulation is frequently computationally expensive because of the high dimensions of the dynamic model of a blade-rotor system. To overcome this problem, a new method that combines the receptance-based dimension-reduction approach with the incremental harmonic balance (IHB) method is presented in this study. First, a dynamic model of a blade-rotor system is developed using the finite element method, and the number of dimensions of the model is reduced by the receptance method. Subsequently, the steady-state response is obtained by the improved IHB method to conveniently manage the large number of super-harmonic components of the local rubbing system. Finally, the precision and efficiency of the proposed method is verified by comparing its results with those obtained by the Newmark-β method. The proposed method is found to be efficient in analyzing local rubbing blade-rotor systems with high dimensions, local nonlinearities, and rich super-harmonics.

Keywords: Blade-rotor system; Local rubbing; Steady-state response; Incremental harmonic balance method; Receptance-based dimension reduction

1. Introduction

The blade-rotor system is an important component of turbomachinery (e.g., steam turbines, aeroengines, and air compressors). Blade-to-case local rubbing faults frequently occur because of the small clearance between the blade and the case. These faults can seriously affect the safe and stable operation of rotating machinery. In the past decades, numerous studies have been conducted on rubbing blade-rotor systems, as presented in the comprehensive review of Muszynska [1].

In general, the dynamic model of a blade-rotor system in large rotating machinery has high dimensions and strong nonlinearity. Therefore, a numerical simulation instead of an analytical method is commonly used to predict response in such systems. However, using numerical methods such as the Newmark-β [2, 3] and the Runge-Kutta [4] to analyze high-dimensional dynamic systems, particularly blade-to-case rubbing rotor systems, is time-consuming. To overcome this disadvantage, reducing the number of dimensions of nonlinear blade-rotor systems is critical. At present, two types of approach are available to reduce the dimensions of such dynamic systems with a large number of degrees of freedom (DOFs). The first type is the dynamic substructure methods, which are frequently combined with time-domain methods. The fixed-interface component mode synthesis (CMS) approach [5-7] is the most widely used dynamic substructure method. In this method, the structure is divided into two parts (linear and nonlinear parts). Modal truncation is applied to the linear part, and only the lower-order modes remain; therefore, the number of dimensions of the initial structure is reduced. Although these methods can reduce computational effort, the accuracy of the result may decrease because the effects of higher-order modes are ignored [8].

The second type comprises receptance-based dimension-reduction approaches [9, 10], which are frequently combined with frequency-domain methods. By utilizing the receptance functions of the linear part of a system, the number of dimensions can be reduced to be equal to that of nonlinear DOFs. Therefore, this method can significantly improve computational efficiency for steady-state response prediction. In addition, it is more accurate than the CMS method because it avoids modal truncations.

In some studies, the receptance-based dimension-reduction method was combined with the harmonic balance (HB) method [11] and the describing function (DF) method [12] to obtain the steady-state response of local nonlinear systems. For example, Bonellop [13] developed the receptance HB method to rapidly compute the steady-state periodic vibration of an entire aeroengine model. Similar methods were proposed by other researchers [14-16]. Wei and Zheng [8] conducted multi-harmonic response analysis of a dynamic system with local nonlinearities based on the DF method and linear receptance data. All these studies have proven that using the receptance-

*Corresponding author. Tel.: +86 24 83671429, Fax.: +86 24 83671429
E-mail address: hlyao@mail.neu.edu.cn
† Recommended by Editor Yeon June Kang

based dimension-reduction method before employing frequency-domain analysis methods, such as the HB and DF methods, can greatly improve computational efficiency. However, few studies have utilized the receptance-based dimension-reduction method to expand the applicability of the IHB method.

Blade-to-case rubbing is frequently local to rotating machinery, and a large number of super-harmonics exists in the steady-state responses of the system [17]. These super-harmonics should be considered to achieve precise numerical simulation results. The IHB method [18-23] is an efficient tool for analyzing strong nonlinear vibrations with multi-harmonics. It can also provide solutions with higher precision than the HB and DF methods. Therefore, a new response prediction method based on the IHB method for blade-to-case rubbing is proposed. To reduce the time required for calculation, the method is combined with the receptance-based dimension-reduction approach. Numerical experiments are performed to verify the precision and efficiency of the proposed method.

2. Dynamic modeling of a blade-rotor system

2.1 Dynamic model

The structure of a blade-rotor system is frequently complicated; hence, modeling the system using commercial finite element software such as ANSYS is convenient. Analyzing the system by using finite element discretization to conveniently find a solution is necessary.

In the following subsection, the finite element model of each part of the blade-rotor system is developed using the ANSYS Parametric Design Language.

2.1.1 Rotor beam element model

In the rotor system, the rotor shaft can be discretized into Beam188 elements. Each node of the beam element has three translational and three rotational DOFs, as shown in Fig. 1. The generalized displacement of each element is defined by Eq. (1):

$$\left[x_A, y_A, z_A, \theta_{xA}, \theta_{yA}, \theta_{zA}, x_B, y_B, z_B, \theta_{xB}, \theta_{yB}, \theta_{zB}\right]^T. \quad (1)$$

2.1.2 Blade shell element model

The blade is modeled using the Shell63 element, which has both bending and membrane capabilities. The element has 6 DOFs at each node: translations in the nodal *x*, *y*, and *z* directions and rotations about the nodal *x*, *y*, and *z* axes. The geometric model of this element is presented in Fig. 2.

2.1.3 Support and connection

The left and right supports of the rotor system are modeled using the Matrix27 element. The connection between the rotor and the blade roots is considered to be rigid, and the "CERIG" command in ANSYS is used to connect the two types of element (The rotor and the blade).

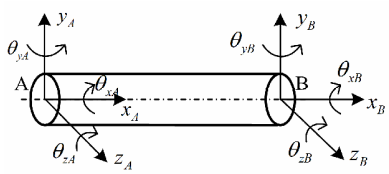

Fig. 1. Model of the beam element.

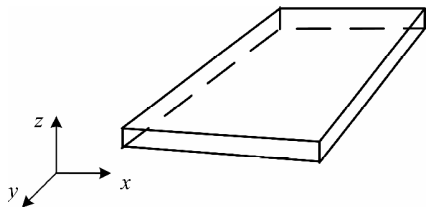

Fig. 2. Model of the shell element.

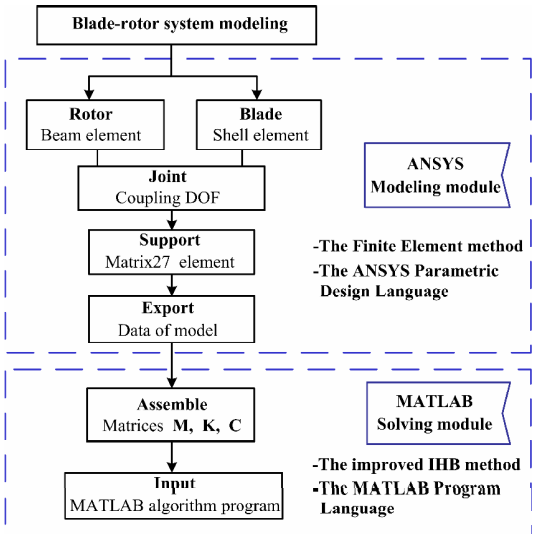

Fig. 3. Complete modeling procedure of the blade-rotor system.

Thus, the dynamic modeling of the blade-rotor system is completed and the following assumptions are accounted for.

(1) Straight blades are adopted in this model, and the effect of blade profile is neglected.

(2) The connection between the blade roots and the disk is rigid coupling that neglects the contact of tenon/mortise.

2.2 Dynamic modeling procedure

Although model development is convenient using ANSYS, solving the problem of local rubbing nonlinear vibration and obtaining a steady-state response using this software is difficult and time-consuming. Therefore, finite element model data are exported to MATLAB to develop the mathematical model and solve the problem.

The exported data are assembled into matrices **M**, **K**, and **C** using matrix assembly techniques. These matrices are entered into the MATLAB algorithm program to conveniently find a solution for the system. The entire modeling procedure of the

blade-rotor system (Fig. 3) is divided into two modules, namely: the ANSYS modeling module and the MATLAB solving module.

2.3 Mathematical model

While considering the effect of nonlinear rubbing, the equation of motion of the blade-to-case contact rotor system is given in Eq. (2):

$$\mathbf{M}\ddot{\mathbf{x}} + \mathbf{C}\dot{\mathbf{x}} + \mathbf{K}\mathbf{x} = \mathbf{U} + \mathbf{F}_r \,, \tag{2}$$

where $\mathbf{M}$, $\mathbf{C}$, and $\mathbf{K}$ are the mass, damping, and stiffness matrices, respectively; $\mathbf{x}$ is the displacement vector; $\mathbf{U}$ is the excitation vector caused by unbalance; and $\mathbf{F}_r$ is the nonlinear rubbing force vector. The dots above $\mathbf{x}$ denote differentiation with respect to time t.

Assuming that rubbing occurs at node *l*, the rubbing force vector can be written as shown in Eq. (3):

$$\mathbf{F}_r = \left[\overbrace{0,\cdots,0}^{6l-6} \quad f_{nx} \quad f_{ny} \quad 0,\cdots,0 \right]^{\mathrm{T}} , \tag{3}$$

where f_{nx} and f_{ny} are the rubbing force components in the *x* and *y* directions, respectively.

The rubbing force adopts the model of piecewise linear nonlinearity and the expressions are given in Eq. (4):

$$\begin{aligned} f_{ni}\left(x_{J_i}\right) &= \begin{cases} k_{ni}\left(x_{J_i} - e_i\right), & x_{J_i} \ge e_i \\ k_{ni}\left(x_{J_i} + e_i\right), & x_{J_i} \le -e_i \end{cases} \quad (i = 1,2,3\cdots), \\ f_{ni}\left(x_{J_i}\right) &= 0 , \qquad\qquad -e < x_{J_i} < e_i \end{aligned} \tag{4}$$

where, f_{ni} is the nonlinear force at node *i*, x_{J_i} is the radial displacement, k_{ni} represents the nonlinear contact stiffness, and e_i denotes the clearance between the blades and the case. The blade tip comes in contact with the case when its radial vibration exceeds clearance e_i.

3. Methodological details

3.1 Dimension reduction based on receptance data

The DOFs of the rotor system are separated into two distinct groups, namely: the nonlinear group $\mathbf{x}_1$ contains DOFs that are related to nonlinear rubbing forces, and the linear group $\mathbf{x}_2$ contains DOFs that are unrelated to rubbing forces.

Eq. (2) can be rearranged as follows:

$$\mathbf{M}\ddot{\mathbf{x}} + \mathbf{C}\dot{\mathbf{x}} + \mathbf{K}\mathbf{x} + \mathbf{f}_n\left(\mathbf{x},\dot{\mathbf{x}}\right) = \mathbf{F}_1 \cos\omega t + \mathbf{F}_2 \sin\omega t \,; \tag{5}$$

that is,

$$\begin{aligned} &\begin{bmatrix} \mathbf{M}_{11} & \mathbf{M}_{12} \\ \mathbf{M}_{21} & \mathbf{M}_{22} \end{bmatrix} \begin{Bmatrix} \ddot{\mathbf{x}}_1 \\ \ddot{\mathbf{x}}_2 \end{Bmatrix} + \begin{bmatrix} \mathbf{C}_{11} & \mathbf{C}_{12} \\ \mathbf{C}_{21} & \mathbf{C}_{22} \end{bmatrix} \begin{Bmatrix} \dot{\mathbf{x}}_1 \\ \dot{\mathbf{x}}_2 \end{Bmatrix} + \begin{bmatrix} \mathbf{K}_{11} & \mathbf{K}_{12} \\ \mathbf{K}_{21} & \mathbf{K}_{22} \end{bmatrix} \begin{Bmatrix} \mathbf{x}_1 \\ \mathbf{x}_2 \end{Bmatrix} \\ &+ \begin{Bmatrix} \mathbf{f}_{n1}\left(\mathbf{x}_1,\dot{\mathbf{x}}_1\right) \\ 0 \end{Bmatrix} = \begin{Bmatrix} \mathbf{F}_{11} \\ \mathbf{F}_{21} \end{Bmatrix} \cos\omega t + \begin{Bmatrix} \mathbf{F}_{12} \\ \mathbf{F}_{22} \end{Bmatrix} \sin\omega t \end{aligned} . \tag{6}$$

When the rotor system is in a steady state, the response vector $\mathbf{x}$ is periodic, and the response of node *i* can be expanded as follows:

$$x_i = a_{0i} + \sum_{k=1}^{r} \left(a_{ki} \cos(k\omega t) + b_{ki} \sin(k\omega t) \right) = \mathbf{C}_s \mathbf{A}_i \,, \tag{7}$$

where $\mathbf{C}_s = \begin{bmatrix} 1 & \cos\omega t & \sin\omega t & \cdots & \cos r\omega t & \sin r\omega t \end{bmatrix}$ and $\mathbf{A}_i = \begin{bmatrix} a_{0i} & a_{1i} & b_{1i} & \cdots & a_{ri} & b_{ri} \end{bmatrix}^{\mathrm{T}}$.

If $\mathbf{S} = \mathrm{diag}\left[\mathbf{C}_s, \mathbf{C}_s, \cdots, \mathbf{C}_s\right]$ and $\mathbf{A} = \left[\mathbf{A}_1^{\mathrm{T}}, \mathbf{A}_2^{\mathrm{T}}, \cdots, \mathbf{A}_h^{\mathrm{T}}\right]^{\mathrm{T}}$, then $\mathbf{x} = \mathbf{S}\mathbf{A}$.

When the rotor system is in a steady state, the nonlinear force vector $\mathbf{f}_n\left(\mathbf{x},\dot{\mathbf{x}}\right)$ is also periodic and can be expressed as follows:

$$\mathbf{f}_n\left(\mathbf{x},\dot{\mathbf{x}}\right) = \mathbf{S}\mathbf{P} \,, \tag{8}$$

where $\mathbf{P} = \left[\mathbf{P}_1^{\mathrm{T}}, \mathbf{P}_2^{\mathrm{T}}, \cdots, \mathbf{P}_h^{\mathrm{T}}\right]^{\mathrm{T}}$, $\mathbf{P}_i = \left[p_{0i}, p_{1i}, q_{1i}, \cdots, p_{ri}, q_{ri}\right]^{\mathrm{T}}$.

Suppose that $\bar{\mathbf{x}} = \mathbf{S}_e\mathbf{A}$, $\mathbf{C}_{se} = \left[1, \mathrm{e}^{\mathrm{j}\omega t}, \mathrm{je}^{-\mathrm{j}\omega t}, \cdots, \mathrm{e}^{\mathrm{j}r\omega t}, \mathrm{je}^{-\mathrm{j}r\omega t}\right]$, and $\mathbf{S}_e = \mathrm{diag}\left[\mathbf{C}_{se}, \mathbf{C}_{se}, \cdots, \mathbf{C}_{se}\right]$. Then, $\mathbf{x} = \mathrm{Re}\left(\bar{\mathbf{x}}\right)$ and $\bar{\mathbf{x}}$ satisfy the following equation:

$$\mathbf{M}\ddot{\bar{\mathbf{x}}} + \mathbf{C}\dot{\bar{\mathbf{x}}} + \mathbf{K}\bar{\mathbf{x}} + \bar{\mathbf{f}}_n = \mathbf{F}_1 \mathrm{e}^{\mathrm{j}\omega t} + \mathrm{j}\mathbf{F}_2 \mathrm{e}^{-\mathrm{j}\omega t} \,, \tag{9}$$

where $\bar{\mathbf{f}}_n = \mathbf{S}_e\mathbf{P}$ and $\mathbf{f}_n = \mathrm{Re}\left(\bar{\mathbf{f}}_n\right)$.

Eq. (9) can be rewritten as follows:

$$\begin{aligned} &\begin{bmatrix} \mathbf{M}_{11} & \mathbf{M}_{12} \\ \mathbf{M}_{21} & \mathbf{M}_{22} \end{bmatrix} \begin{Bmatrix} \ddot{\bar{\mathbf{x}}}_1 \\ \ddot{\bar{\mathbf{x}}}_2 \end{Bmatrix} + \begin{bmatrix} \mathbf{C}_{11} & \mathbf{C}_{12} \\ \mathbf{C}_{21} & \mathbf{C}_{22} \end{bmatrix} \begin{Bmatrix} \dot{\bar{\mathbf{x}}}_1 \\ \dot{\bar{\mathbf{x}}}_2 \end{Bmatrix} + \begin{bmatrix} \mathbf{K}_{11} & \mathbf{K}_{12} \\ \mathbf{K}_{21} & \mathbf{K}_{22} \end{bmatrix} \begin{Bmatrix} \bar{\mathbf{x}}_1 \\ \bar{\mathbf{x}}_2 \end{Bmatrix} . \\ &+ \begin{Bmatrix} \bar{\mathbf{f}}_{n1} \\ 0 \end{Bmatrix} = \begin{Bmatrix} \mathbf{F}_{11} \\ \mathbf{F}_{21} \end{Bmatrix} \mathrm{e}^{\mathrm{j}\omega t} + \mathrm{j} \begin{Bmatrix} \mathbf{F}_{12} \\ \mathbf{F}_{22} \end{Bmatrix} \mathrm{e}^{-\mathrm{j}\omega t} \end{aligned} \tag{10}$$

Suppose $\bar{\mathbf{x}} = \sum_{k=0}^{r} \bar{\mathbf{x}}_{Hk}$, where $\bar{\mathbf{x}}_k = \left[\bar{x}_{H1k}, \bar{x}_{H2k}, \cdots, \bar{x}_{HNk}\right]$ is the *k*th-order harmonic term of response $\bar{\mathbf{x}}$, and $\bar{x}_{Hik} = p_{ik}\mathrm{e}^{\mathrm{j}k\omega t} + \mathrm{j}q_{ik}\mathrm{e}^{-\mathrm{j}k\omega t}$. Based on the second term of Eq. (10), the *k*th harmonic term $\bar{\mathbf{x}}_{H2k}$ can be written as follows:

$$\begin{aligned} \bar{\mathbf{x}}_{H2k} = &-\left(\mathbf{K}_{22} - \mathbf{M}_{22}k^2\omega^2 + \mathrm{j}\mathbf{C}_{22}k\omega\right)^{-1} \\ &\times \left(\mathbf{K}_{21} - \mathbf{M}_{21}k^2\omega^2 + \mathrm{j}\mathbf{C}_{21}k\omega\right)\bar{\mathbf{x}}_{H1k} \end{aligned} . \tag{11}$$

Substituting Eq. (11) into the first term of Eq. (10) yields

$$\mathbf{M}_{ek}\ddot{\bar{\mathbf{x}}}_{H1k}+\mathbf{C}_{ek}\dot{\bar{\mathbf{x}}}_{H1k}+\mathbf{K}_{ek}\bar{\mathbf{x}}_{H1k}+\bar{\mathbf{f}}_{Hn1k}=0\,, \tag{12}$$

where $\bar{\mathbf{f}}_{Hn1k}$ is the kth harmonic term of $\bar{\mathbf{f}}_{n1}$,

$$\begin{aligned}\mathbf{M}_{ek}&=\mathbf{M}_{11}-\mathbf{M}_{12}\left(\mathbf{K}_{22}-\mathbf{M}_{22}k^2\omega^2+\mathrm{j}\mathbf{C}_{22}k\omega\right)^{-1}\\&\quad\times\left(\mathbf{K}_{21}-\mathbf{M}_{21}k^2\omega^2+\mathrm{j}\mathbf{C}_{21}k\omega\right)\\\mathbf{C}_{ek}&=\mathbf{C}_{11}-\mathbf{C}_{12}\left(\mathbf{K}_{22}-\mathbf{M}_{22}k^2\omega^2+\mathrm{j}\mathbf{C}_{22}k\omega\right)^{-1}\\&\quad\times\left(\mathbf{K}_{21}-\mathbf{M}_{21}k^2\omega^2+\mathrm{j}\mathbf{C}_{21}k\omega\right)\\\mathbf{K}_{ek}&=\mathbf{K}_{11}-\mathbf{K}_{12}\left(\mathbf{K}_{22}-\mathbf{M}_{22}k^2\omega^2+\mathrm{j}\mathbf{C}_{22}k\omega\right)^{-1}\\&\quad\times\left(\mathbf{K}_{21}-\mathbf{M}_{21}k^2\omega^2+\mathrm{j}\mathbf{C}_{21}k\omega\right)\end{aligned}.$$

For the fundamental harmonic term $\bar{\mathbf{x}}_{H1}$, if $\bar{\mathbf{x}}_L=\left(\mathbf{K}-\omega^2\mathbf{M}+\mathrm{j}\omega\mathbf{C}\right)^{-1}\mathbf{F}_1\mathrm{e}^{\mathrm{j}\omega t}+\left(\mathbf{K}-\omega^2\mathbf{M}-\mathrm{j}\omega\mathbf{C}\right)^{-1}\mathrm{j}\mathbf{F}_2\mathrm{e}^{-\mathrm{j}\omega t}$ is the response of a rotor system with no rubbing, and if $\bar{\mathbf{x}}_{H1}=\bar{\mathbf{x}}_L+\Delta\bar{\mathbf{x}}_{H1}$, then $\Delta\bar{\mathbf{x}}_{H1}$ satisfies the following equation:

$$\mathbf{M}\Delta\ddot{\bar{\mathbf{x}}}_{H1}+\mathbf{C}\Delta\dot{\bar{\mathbf{x}}}_{H1}+\mathbf{K}\Delta\bar{\mathbf{x}}_{H1}+\bar{\mathbf{f}}_{Hn1}=0\,. \tag{13}$$

From Eq. (13), the following equation can be obtained:

$$\begin{aligned}&\mathbf{M}_{e1}\ddot{\bar{\mathbf{x}}}_{H11}+\mathbf{C}_{e1}\dot{\bar{\mathbf{x}}}_{H11}+\mathbf{K}_{ek}\bar{\mathbf{x}}_{H11}+\bar{\mathbf{f}}_{Hn11}\\&=\mathbf{M}_{e1}\ddot{\bar{\mathbf{x}}}_{L1}+\mathbf{C}_{e1}\dot{\bar{\mathbf{x}}}_{L1}+\mathbf{K}_{ek}\bar{\mathbf{x}}_{L1}\end{aligned}. \tag{14}$$

From Eqs. (12) and (14), the following equation can be derived:

$$\begin{aligned}&\sum_{k=0}^{r}\mathbf{M}_{ek}\ddot{\bar{\mathbf{x}}}_{\mathrm{H}1k}+\sum_{k=0}^{r}\mathbf{C}_{ek}\dot{\bar{\mathbf{x}}}_{\mathrm{H}1k}+\sum_{k=0}^{r}\mathbf{K}_{ek}\bar{\mathbf{x}}_{\mathrm{H}1k}+\bar{\mathbf{f}}_{\mathrm{n}}\\&=\mathbf{M}_{e1}\ddot{\bar{\mathbf{x}}}_{1L}+\mathbf{C}_{e1}\dot{\bar{\mathbf{x}}}_{1L}+\mathbf{K}_{e1}\bar{\mathbf{x}}_{1L}\end{aligned}. \tag{15}$$

The number of dimensions of Eq. (15) is considerably less than that of the original system. Moreover, Eq. (15) only considers the nonlinear forces because the responses of the linear part are already represented in the responses of the nonlinear part by using the frequency response function (Receptance).

The real part of Eq. (15) can be written as follows:

$$\begin{aligned}&\mathrm{Re}\left(\sum_{k=0}^{r}\mathbf{M}_{ek}\ddot{\bar{\mathbf{x}}}_{H1k}+\sum_{k=0}^{r}\mathbf{C}_{ek}\dot{\bar{\mathbf{x}}}_{H1k}+\sum_{k=0}^{r}\mathbf{K}_{ek}\bar{\mathbf{x}}_{H1k}\right)\\&+\mathbf{f}_n\left(\mathbf{x},\dot{\mathbf{x}}\right)=\mathrm{Re}\left(\mathbf{M}_{e1}\ddot{\bar{\mathbf{x}}}_{1L}+\mathbf{C}_{e1}\dot{\bar{\mathbf{x}}}_{1L}+\mathbf{K}_{e1}\bar{\mathbf{x}}_{1L}\right)\end{aligned}. \tag{16}$$

Eq. (16) can be solved by the IHB method. After $\bar{\mathbf{x}}_1$ is obtained, $\bar{\mathbf{x}}_2$ can be recovered from $\bar{\mathbf{x}}_1$ using Eq. (11).

3.2 Receptance IHB method

The IHB method is an effective method for obtaining periodic solutions to nonlinear multi-DOF systems. A brief introduction to the procedures of the method is presented in this paper; further details can be found in Refs. [18-23].

The general form of the equation with real number parameters is given by Eq. (17):

$$\mathbf{M}\ddot{\mathbf{x}}+\mathbf{C}\dot{\mathbf{x}}+\mathbf{K}\mathbf{x}+\mathbf{f}_n\left(\mathbf{x}\right)=\mathbf{F}_1\cos\omega t+\mathbf{F}_2\sin\omega t\,. \tag{17}$$

Assuming that the periodic solution is $\mathbf{x}=\mathbf{S}\mathbf{A}$, and

$$\mathbf{x}=\mathbf{x}_0+\varepsilon\mathbf{x}\,; \tag{18}$$

then $\mathbf{x}_0=\mathbf{S}\mathbf{A}_0$ and $\varepsilon\mathbf{x}=\mathbf{S}\varepsilon\mathbf{A}$.

By substituting Eq. (18) into Eq. (17) and neglecting higher-order harmonic components, the following equation is obtained:

$$\begin{aligned}&\mathbf{M}\ddot{\mathbf{S}}\varepsilon\mathbf{A}+\mathbf{C}\dot{\mathbf{S}}\varepsilon\mathbf{A}+\mathbf{K}\mathbf{S}\varepsilon\mathbf{A}+\mathbf{C}_n\dot{\mathbf{S}}\varepsilon\mathbf{A}+\mathbf{K}_n\mathbf{S}\varepsilon\mathbf{A}=-\\&\left(\mathbf{M}\ddot{\mathbf{S}}\mathbf{A}_0+\mathbf{C}\dot{\mathbf{S}}\mathbf{A}_0+\mathbf{K}\mathbf{S}\mathbf{A}_0\right)+\mathbf{F}_1\cos\omega t+\mathbf{F}_2\sin\omega t-\mathbf{f}_n\left(\mathbf{x}_0\right)\end{aligned}, \tag{19}$$

where $\mathbf{K}_n=\dfrac{\partial\mathbf{f}_n}{\partial\mathbf{x}}$ and $\mathbf{C}_n=\dfrac{\partial\mathbf{f}_n}{\partial\dot{\mathbf{x}}}$.

By applying Galerkin's procedure, Eq. (19) yields

$$\begin{aligned}&\int_0^{2\pi/\omega}\mathbf{S}^{\mathrm{T}}\left(\mathbf{M}\ddot{\mathbf{S}}+\mathbf{C}\dot{\mathbf{S}}+\mathbf{K}\mathbf{S}+\mathbf{C}_n\dot{\mathbf{S}}+\mathbf{K}_n\mathbf{S}\right)\mathrm{d}t\cdot\varepsilon\mathbf{A}\\&=-\int_0^{2\pi/\omega}\mathbf{S}^{\mathrm{T}}\left(\mathbf{M}\ddot{\mathbf{S}}+\mathbf{C}\dot{\mathbf{S}}+\mathbf{K}\mathbf{S}\right)\mathrm{d}t\cdot\mathbf{A}_0\\&+\int_0^{2\pi/\omega}\mathbf{S}^{\mathrm{T}}\left[\mathbf{F}_1\cos\omega t+\mathbf{F}_2\sin\omega t-\mathbf{f}_n\left(\mathbf{x}_0\right)\right]\mathrm{d}t\end{aligned}. \tag{20}$$

Through iteration, $\mathbf{A}$ can be solved first from Eq. (20), and then $\mathbf{x}$ can be calculated afterward.

The difference between Eqs. (15) and (17) is that the coefficients in Eq. (15) are complex numbers, and thus, the IHB method cannot be used directly. To improve the IHB method, suppose that

$$\begin{cases}\mathbf{C}_{se0}=\left[\begin{array}{cc}1&\overbrace{0\cdots0}^{2r}\end{array}\right]\\\mathbf{C}_{sek}=\left[\begin{array}{ccccc}1&\overbrace{0\cdots0}^{2(k-1)}&\mathrm{e}^{\mathrm{j}k\omega t}&-\mathrm{j}\mathrm{e}^{\mathrm{j}k\omega t}&\overbrace{0\cdots0}^{2(r-k)}\end{array}\right]\quad k>0\end{cases}. \tag{21}$$

$$\mathbf{S}_{ek}=\begin{bmatrix}\mathbf{C}_{sek}&&&\\&\mathbf{C}_{sek}&&\\&&\cdots&\\&&&\mathbf{C}_{sek}\end{bmatrix}\quad k=0\cdots r\,. \tag{22}$$

Table 1. Rotor element parameters.

Serial number	1	2	3	4	5	6	7	8	9	10	11	12	13	14
Length (mm)	287	259	337	175	175	37	54	54	294	54	54	294	54	54
Diameter (mm)	184	225	310	340	340	448	600	600	448	600	600	448	600	600
Serial number	15	16	17	18	19	20	21	22	23	24	25	26	27	28
Length (mm)	294	54	54	360	150	100	140	100	150	199.5	199.5	225	180	617
Diameter (mm)	448	600	600	486	400	1007	400	1007	400	370	370	225	196	170

Based on Eq. (12), the following deduction can be made:

$$\begin{aligned}&\int_0^{2\pi/\omega}\mathbf{S}^{\mathrm{T}}\,\mathrm{Re}\sum_{k=0}^{r}\begin{pmatrix}\mathbf{M}_{ek}\ddot{\mathbf{S}}_{ek}+\mathbf{C}_{ek}\dot{\mathbf{S}}_{ek}+\mathbf{K}_{ek}\mathbf{S}_{ek}\\+\mathrm{C}_n\dot{\mathbf{S}}+\mathbf{K}_n\mathbf{S}\end{pmatrix}\mathrm{d}t\cdot\varepsilon\mathbf{A}\\&=-\int_0^{2\pi/\omega}\mathbf{S}^{\mathrm{T}}\,\mathrm{Re}\sum_{k=0}^{r}\left(\mathbf{M}_{ek}\ddot{\mathbf{S}}_{ek}+\mathbf{C}_{ek}\dot{\mathbf{S}}_{ek}+\mathbf{K}_{ek}\mathbf{S}_{ek}\right)\mathrm{d}t\cdot\mathbf{A}_0\ .\\&+\int_0^{2\pi/\omega}\mathbf{S}^{\mathrm{T}}\begin{bmatrix}\mathrm{Re}\left(\mathbf{M}_{e1}\ddot{\mathbf{x}}_{1L}\right)+\mathrm{Re}\left(\mathbf{C}_{e1}\dot{\mathbf{x}}_{1L}\right)\\+\mathrm{Re}\left(\mathbf{K}_{e1}\mathbf{x}_{1L}\right)-\mathbf{f}_n\left(\mathbf{x}_0,\dot{\mathbf{x}}_0\right)\end{bmatrix}\mathrm{d}t\end{aligned}\qquad(23)$$

Therefore,

$$\mathbf{K}_m\Delta\mathbf{A}=\mathbf{R}_{m1}\mathbf{A}_0+\mathbf{R}_{m2}\ .\qquad(24)$$

Through iteration, $\mathbf{A}_0$ can be solved from Eq. (24); and finally, $\mathbf{x}$ can be obtained.

4. Numerical experiments and discussion

4.1 Introduction to the blade-rotor system

The dynamic model of the rotor system with blade-to-case rubbing is displayed in Fig. 4. The rotor is divided into 28 segments and 29 nodes, and the element parameters are listed in Table 1.

Four groups of blades, with eight blades in each group, are rigidly connected with the rotor system. The geometric and material parameters of the blades are listed in Table 2.

The left and right supports depicted in Fig. 4 are located at nodes 5 and 26, respectively, with a support stiffness of 5×10^9 N/m. Assuming that the elastic modulus of steel is 210 GPa, the density of the rotor material is 7850 kg/m^3.

The finite element model is shown in Fig. 5, in which several key nodes used in the following numerical simulations are indicated. In this study, the rubbing fault is assumed to occur at node 10198 (a blade tip on the fourth blade group) and the excitation force is imposed on node 17, as illustrated in Fig. 5. The finite element model has 1710 and 1326 DOFs before and after coupling DOF, respectively.

4.2 Precision comparison

4.2.1 Comparison with the Newmark-β method

The excitation force (Amplitude $A = 1\times10^4$ N, frequency f = 20 Hz) is imposed at node 17 in the rotor, with the nonlinear contact stiffness and rubbing clearance values of $k_n = 1\times10^9$ N/m and $e = 4\times10^{-4}$ m, respectively.

Table 2. Geometric and material parameters of the blade.

Width of the blade (mm)	90
Height of the blade (mm)	180
Thickness of the blade (mm)	10
Elastic modulus (GPa)	210
Material density (kg·m^{-3})	7850
Poisson's ratio	0.3

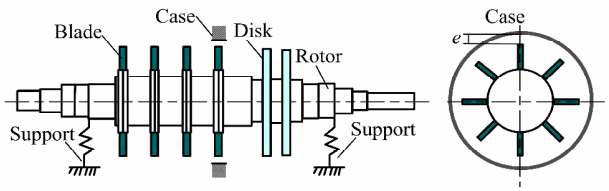

Fig. 4. Dynamic model of the rotor system with blade-to-case rubbing.

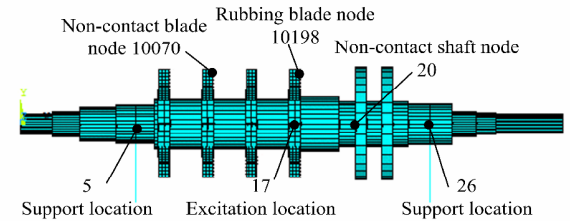

Fig. 5. 1326-DOF finite element model of the blade-rotor system.

The comparison of the steady-state responses obtained from these two methods is depicted in Fig. 6, wherein the solid lines denote the results of the Newmark-β method and the solid lines with "○" represent the results of the proposed method. In particular, Figs. 6(a) and (b) show the conditions under symmetric and asymmetric rubbing, respectively. The comparison of the proposed method with the Newmark-β method shows that their calculated results are nearly identical. Hence, the precision of the proposed method is verified.

4.2.2 Steady-state responses at different locations

The steady-state responses at the noncontact node 10070 on the blade and at node 20 on the shaft are illustrated in Figs. 7(a)-(d), with the same simulation parameters as those in Fig. 6. The response of the noncontact location on the blade has similar characteristics to the rubbing location on the blade,

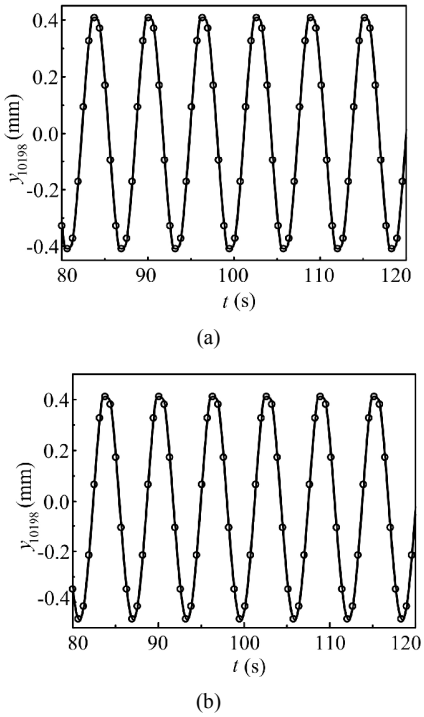

Fig. 6. Comparison of the steady-state responses of y_{10198} obtained by the proposed method and the Newmark-β method.

whereas the response of the blade is slightly more nonlinear than that of the location on the shaft. This result indicates that the proposed method can obtain the responses of both nonlinear and linear locations.

4.2.3 Multi-harmonic responses for different contact stiffness values

The multi-harmonic curves at rubbing node 10198 for excitation frequencies ranging from 10 Hz to 40 Hz with $e = 2\times10^{-4}$ m are shown in Fig. 8. In particular, Figs. 8(a)-(c) represent the condition of asymmetric rubbing with $k_{n1} = 1\times10^{7}$ N/m, $k_{n2} = 5\times10^{7}$ N/m, and $k_{n3} = 1\times10^{8}$ N/m for harmonic components 0X, 1X, and 2X, respectively. Meanwhile, Figs. 8(d)-(f) represent the condition of symmetric rubbing with $k_{n1} = 2\times10^{6}$ N/m, $k_{n2} = 5\times10^{6}$ N/m, and $k_{n3} = 1\times10^{7}$ N/m for harmonic components 1X, 3X, and 5X, respectively. When contact stiffness is large, the proportion of the 1X harmonic component (Fundamental frequency) is small, whereas the proportion of the other harmonic components is large.

4.2.4 Multi-harmonic responses for different rubbing clearances

The multi-harmonic responses at rubbing node 10198 with $e_1 = 2\times10^{-4}$ m, $e_2 = 3\times10^{-4}$ m, and $e_3 = 4\times10^{-4}$ m are presented in Fig. 9. In particular, Figs. 9(a)-(c) denote the condition of asymmetric rubbing with $k_n = 1\times10^{7}$ N/m. In this case, the 1X harmonic component tends to slightly increase, whereas the other harmonic components tend to decrease with the increase in rubbing clearance. In addition, Figs. 9(d)-(f) denote the condition of symmetric rubbing with $k_n = 1\times10^{5}$ N/m. In this case, as rubbing clearance increases, the 1X harmonic component exhibits no obvious change, the peak of the 3X harmonic component tends to increase, the frequency band of the 3X harmonic component becomes narrow, and the peak and frequency band of the 5X harmonic component tend to decrease.

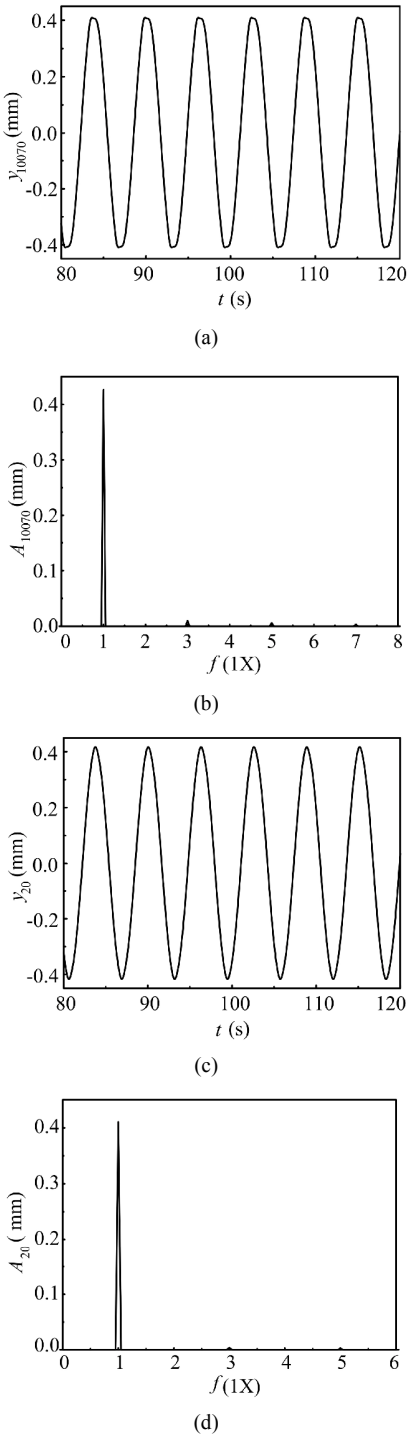

Fig. 7. Time-domain waveforms and amplitude spectrum at nodes 10070 and 20.

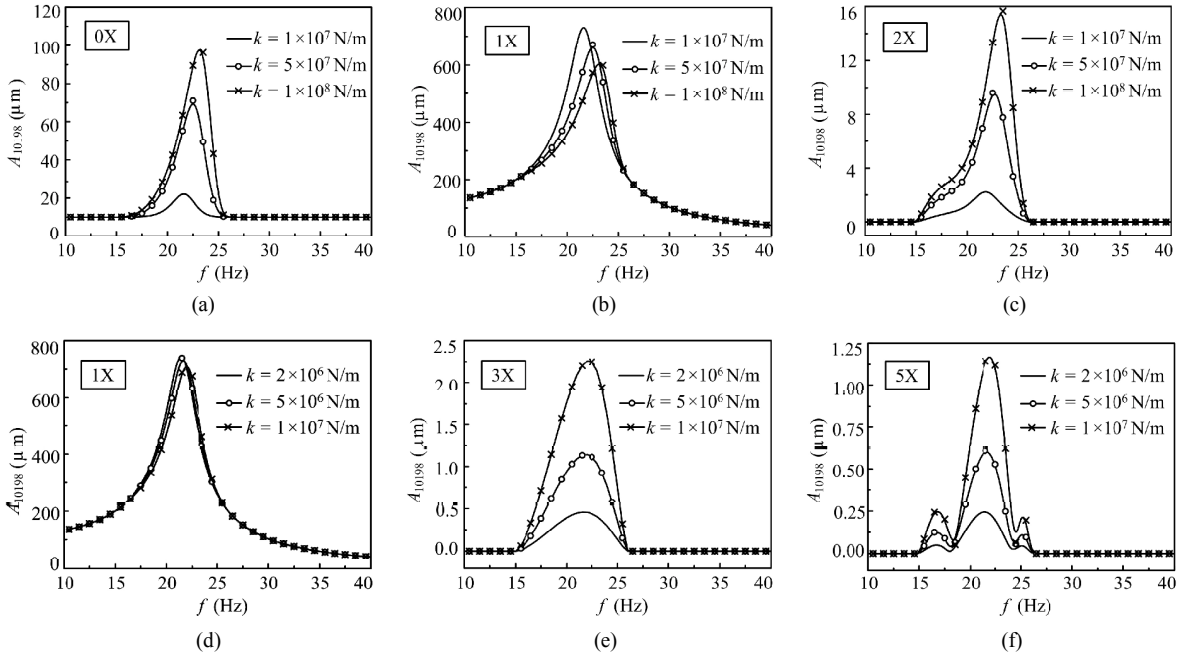

Fig. 8. Multi-harmonic responses with different contact stiffness values.

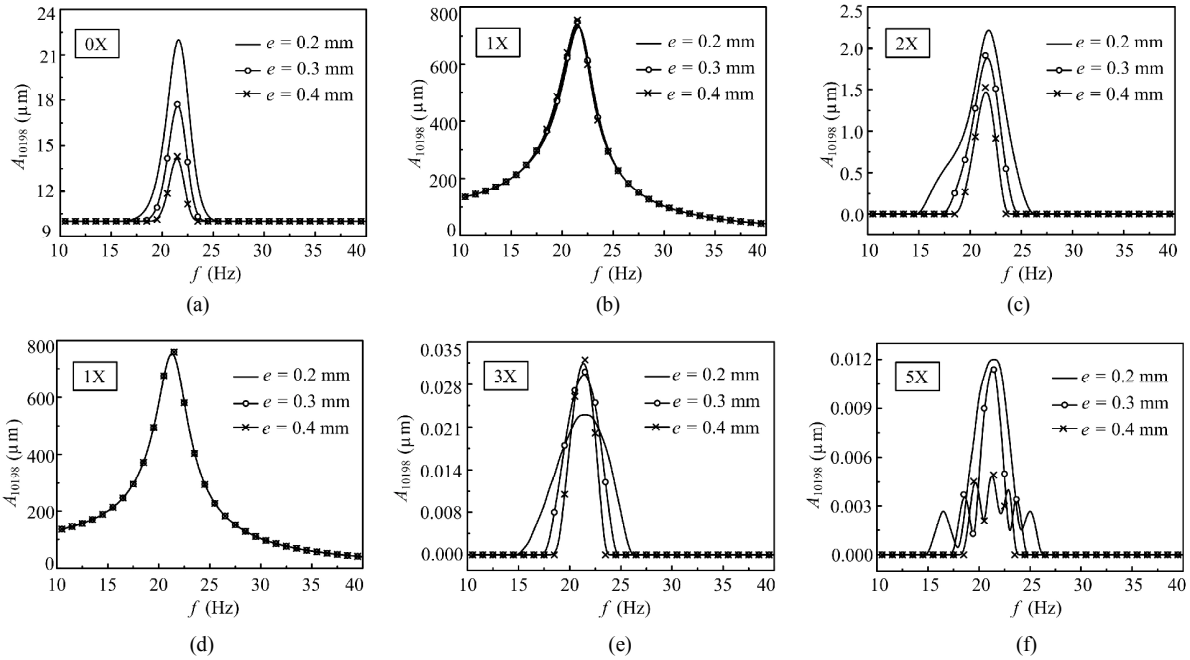

Fig. 9. Multi-harmonic responses with different rubbing clearances.

Based on these analytical results, the effectiveness of the proposed method is confirmed. First, the response at linear locations can be obtained, although the DOFs of the system are reduced to the number of nonlinear DOFs by the reduction method (Fig. 7). Second, the harmonic response can be directly obtained by using the proposed method (Figs. 8 and 9). This finding indicates that the current method is an efficient tool for analyzing the multi-harmonic response of local nonlinear systems.

4.3 Efficiency comparison

To verify the efficiency of the proposed method, its CPU time is compared with that of the Newmark-β method (Table 3). The proposed method can greatly reduce the computational cost of solving the problem. In Table 3, "r" denotes the number of harmonic terms, and "n" represents the number of nonlinear DOFs in the system. Moreover, the effects of these two parameters on computational efficiency are discussed.

Table 3. CPU time of the proposed method and the Newmark-β method.

Method	CPU time (s)
Newmark-β method	36082.280
Proposed method (n = 1, r = 3)	311.304
Proposed method (n = 1, r = 6)	525.362
Proposed method (n = 1, r = 9)	729.784
Proposed method (r = 3, n = 1)	311.695
Proposed method (r = 3, n = 2)	386.441
Proposed method (r = 3, n = 4)	742.415

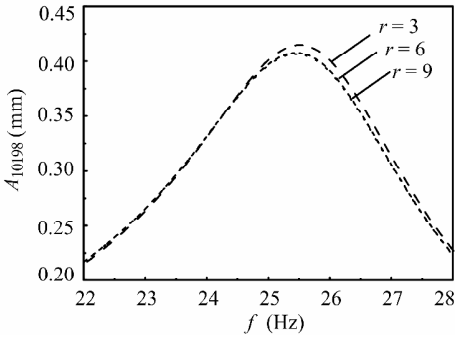

Fig. 10. Influence of the number of harmonic terms on precision.

First, the effect of "r" is investigated. Assuming that one nonlinear DOF exists at node 10198 and taking n = 1 and r = 3, 6, 9, computational cost increases significantly with an increase in the number of harmonic terms r. However, the present method is more economical than the Newmark-β method even when the number of harmonic terms reaches r = 9. The precision of the results is guaranteed when r = 6 (Fig. 10).

Subsequently, the effect of "n" on computational efficiency is studied. Taking r = 3 and n = 1 (Node 10198), n = 2 (Nodes 10198 and 10230, which are uniformly located in one cycle in the fourth blade group at 180°), and n = 4 (Nodes 10198, 10230, 10214, and 10246, which are uniformly located in one cycle in the fourth blade group at 90°), computational efficiency is found to decrease with an increase in the number of nonlinear DOFs, n.

In addition, the effects of these two parameters on the precision of this method are also presented. Based on the HB theory, if more harmonic terms "r" are considered, then more accurate responses can be obtained. Nevertheless, the number of nonlinear DOFs has less influence on the accuracy of the proposed method because the IHB method can analyze both weak and strong nonlinear vibration systems. When the number "n" is large, the nonlinearity of the system is strong.

4.4 Discussion

From the preceding analysis, we can infer that the proposed method is an efficient tool for performing frequency-domain response analysis, which can also be used to directly obtain the harmonic response of each order. Moreover, the proposed method has high efficiency and good precision. It can sharply reduce machine hours compared with the Newmark-β method.

However, the precision and efficiency of the method are also affected by two parameters, namely: the number of harmonic terms adopted and the number of nonlinear DOFs in the system. With an increase in the number of harmonic terms adopted, more accurate results can be obtained but with lower computational efficiency. Moreover, with the increase in the number of nonlinear DOFs, computational efficiency will be reduced.

Thereby, parameter "r" should be selected carefully to find the right balance between precision and efficiency. Provided that precision is assured, the number "r" must be kept to a minimum value to improve the efficiency of the numerical calculation.

5. Conclusion

A blade-rotor system with local rubbing has a large number of super-harmonics and high dimensions. Therefore, a frequency-domain method that combines the IHB and the receptance-based dimension-reduction approach is proposed to obtain the steady-state response of the system.

By comparing the present method with the conventional time-domain method (The Newmark-β method), a conclusion can be drawn that the proposed method can sharply reduce computational effort without compromising the precision of the results. Nevertheless, the proposed method will require more computational effort when the system has more nonlinear DOFs and when more harmonic terms are adopted.

Numerical experiments indicate that the proposed method has excellent advantages for analyzing high-dimensional local nonlinear systems. The method addresses the difficulty in calculating rubbing fault in blade-rotor systems.

Acknowledgement

This work was supported by the National Basic Research Program of China (Grant No. 2011CB706504), the National High Technology Research and Development Program of China (Grant No. 2012AA062002), the graduate student scientific innovation research project (Grant No. N140306003), and the National Natural Science Foundation of China (Grant No. 51475085).

References

[1] A. Muszynska, *Rotor-to-stationary part rubbing contact in rotating machinery*, *Rotordynamics*, CRC Press (2005) 555-710 (Chapter 5).

[2] S. Bouaziz et al., Transient response of a rotor-AMBs system connected by a flexible mechanical coupling, *Mechatronics*, 23 (6) (2013) 573-580.

[3] M. Legrand et al., Two-dimensional modeling of an aircraft

engine structural bladed disk-casing modal interaction, *Journal of Sound and Vibration*, 319 (1-2) (2009) 527-546.

[4] F. L. Chu and Z. S. Zhang, Periodic, quasi-periodic and chaotic vibrations of a rub-impact rotor system supported on oil film bearings, *International Journal of Engineering Science*, 35 (10-11) (1997) 963-973.

[5] S. Kawamura et al., Analysis of nonlinear steady state vibration of a multi-degree-of-freedom system using component mode synthesis method, *Applied Acoustics*, 69 (7) (2008) 624-633.

[6] T. S. Zheng and N. Hasebe, An efficient analysis of high-order dynamical system with local nonlinearity, *Journal of Vibration and Acoustics-Transactions of the ASME*, 121 (3) (1999) 408-416.

[7] D. H. Bae, C. H. Lee and D. S. Bae, Non-linear flexible body analysis for mechanical systems, *Journal of Mechanical Science and Technology*, 26 (7) (2012) 2159-2162.

[8] F. Wei and G. T. Zheng, Multi-harmonic response analysis of systems with local nonlinearities based on describing functions and linear receptance, *Journal of Vibration and Acoustics-Transactions of the ASME*, 132 (2010) 031004-1-031004-6.

[9] Y. Ren and C. F. Beards, A new receptance-based perturbative multi-harmonic balance method for the calculation of the steady state response of non-linear systems, *Journal of Sound and Vibration*, 172 (5) (1994) 593-604.

[10] P. Bonello and H. P. Minh, A receptance harmonic balance technique for the computation of the vibration of a whole aero-engine model with nonlinear bearings, *Journal of Sound and Vibration*, 324 (1) (2009) 221-242.

[11] M. Guskov, J. Sinou and F. Thouverez, Multi-dimensional harmonic balance applied to rotor dynamics, *Mechanics Research Communications*, 35 (8) (2008) 537-545.

[12] A. Gelb and W. E. V. Velde, *Multi-input describing functions and nonlinear system design*, McGraw-Hill, New York (1968).

[13] P. Bonello and P. M. Hai, A receptance harmonic balance technique for the computation of the vibration of a whole aero-engine model with nonlinear bearings, *Journal of Sound and Vibration*, 324 (1-2) (2009) 221-242.

[14] P. Bonello, M. J. Brennan and R. Holmes, Non-linear modeling of rotor dynamic systems with squeeze film dampers-an efficient integrated approach, *Journal of Sound and Vibration*, 249 (4) (2002) 743-773.

[15] P. Bonello, M. J. Brennan and R. Holmes, The prediction of the non-linear dynamics of a squeeze film damped aero-engine rotor housed in a flexible support structure, *Proceedings of the IMechE Part G Journal of Aerospace Engineering*, 218 (3) (2004) 213-230.

[16] Y. Ren and C. F. Beards, A new receptance-based perturbative multi-harmonic balance method for the calculation of the steady state response of non-linear systems, *Journal of Sound and Vibration*, 172 (1994) 593-604.

[17] H. L. Yao et al., Detection of rubbing location in rotor system by super-harmonic responses, *Journal of Mechanical Science and Technology*, 26 (8) (2012) 2431-2437.

[18] S. L. Lau, Y. K. Cheung and S. Y. Wu, A variable parameter incremental method for dynamic instability of linear and nonlinear elastic systems, *Journal of Applied Mechanics of the ASME*, 49 (1982) 849-853.

[19] Y. Shen, S. Yang and X. Liu, Nonlinear dynamics of a spur gear pair with time-varying stiffness and backlash based on incremental harmonic balance method, *International Journal of Mechanical Sciences*, 48 (11) (2006) 1256-1263.

[20] J. X. Zhou and L. Zhang, Incremental harmonic balance method for predicting amplitudes of a multi-d.o.f. non-linear wheel shimmy system with combined Coulomb and quadratic damping, *Journal of Sound and Vibration*, 279 (2005) 403-416.

[21] A. Raghothama and S. Narayanan, Non-linear dynamics of a two-dimensional airfoil by incremental harmonic balance method, *Journal of Sound and Vibration*, 226 (3) (1999) 493-517.

[22] L. Xu, M. W. Lu and Q. Cao, Nonlinear vibrations of dynamical systems with a general form of piecewise linear viscous damping by incremental harmonic balance method, *Physics Letters A*, 301 (2002) 65-73.

[23] K. Y. Sze, S. H. Chen and J. L. Huang, The incremental harmonic balance method for nonlinear vibration of axially moving beams, *Journal of Sound and Vibration*, 281 (2005) 611-626.

Qian Zhao is currently a doctoral candidate at Northeastern University, China. She obtained her B.S. in Mechanical Manufacturing from Hebei Normal University, China in 2011, and her M.S. degree in Mechanical Engineering from Northeastern University, China in 2013. Her research interests include rotor dynamics and nonlinear vibration.

Hongliang Yao is currently an associate professor at Northeastern University, China. He obtained his B.S. degree in 2000 from the Hebei Institute of Technology, China, and his M.S. and Ph.D. degrees in 2003 and 2006, respectively, from Northeastern University, China. His research interests include rotor dynamics and rotating machinery fault diagnosis.